Cavitation and penetration in central collisions with light ions

G. Wang, K. Kwiatkowski, and V. E. Viola
Department of Chemistry and IUCF, Indiana University, Bloomington, Indiana 47405

W. Bauer and P. Danielewicz
Department of Physics and NSCL, Michigan State University, East Lansing, Michigan 48824
(Received 15 September 1995)

The dynamical evolution of central collisions induced by GeV light-ion projectiles is examined with two different Boltzmann-Uehling-Uhlenbeck (BUU) calculations. For projectile energies above 1 GeV incident on heavy target nuclei, a region of depleted density develops in the core of the nucleus at times of the order of 30 fm/c, producing hot residues with significantly depleted density at longer times. The simulations predict penetration of the target by the projectile momentum front at incident energies near 4–6 GeV, leading to a saturation of deposition energy. These results are examined in the context of marked changes in reaction observables reported for light-ion-induced collisions.

PACS number(s): 25.75.−q, 21.65.+f, 24.10.Cn, 25.70.Pq

I. INTRODUCTION

The behavior of hot heavy residues formed in central collisions between light-ion (H and He) projectiles and heavy target nuclei changes markedly as the beam energy increases from 1 to 10 GeV [1,2]. One of the most prominent signals for this transition is the rapid growth (by a factor of $\sim 10^2$) in the probability for complex fragment emission [1–4]. Over this same energy interval, the total N-N scattering cross section remains approximately constant, although the ratio of inelastic-to-elastic collisions increases rapidly and the angular distributions become strongly forward peaked [5]. Exclusive studies have shown that the observed increase is associated with an enhanced probability for multifragmentation of the target residue, and further, have provided evidence for fragment emission from an extended source with $\rho/\rho_0 < 1/3$ [6,7]. Above a beam energy of ~ 8–10 GeV, fragment cross sections become independent of energy and the mass distributions cease to vary (limiting fragmentation [4,6,8]), suggesting that the target nucleus has become transparent to further energy deposition. For beams of heavier projectiles, the onset of constant intermediate-mass-fragment charge distributions occurs at much lower bombarding energies [9].

It is also over the 1–10 GeV bombarding energy region that the inclusive angular distributions for complex fragments evolve from forward to sideways peaked with respect to the beam axis [10,11]. Related studies have shown that fissionlike events detected transverse to the beam direction exhibit anomalously high kinetic energies relative to fission TKE systematics, suggesting a fast breakup of the residue from a compact scission configuration [12].

Large projectile energy loss, or stopping, in $p+A$ reactions has been studied in this energy region as well [13,14]. More relevant to the eventual fate of the targetlike remnant is the question of deposited excitation energy; i.e., the energy that is available to drive the disintegration of the system. Recently, measurements with a 4π detector array have provided evidence for deposition energy saturation in the vicinity of 4 GeV for the ^{3}He+Ag system [15]. Similar conclusions have been reported on the basis of emulsion studies with GeV proton and alpha-particle beams [16]. Above this energy, there is an increase in the number of energetic shower particles, but little change in observables that reflect deposition energy. This may be related to the increasingly forward-focused nature of N-N scattering and higher pion momenta associated with increasing incident energy, thereby enhancing transparency for hadrons in the nuclear medium. It may also be associated with a possible type of Leidenfrost effect in nuclear matter. Thus, questions of both energy deposition and geometry imposed by the reaction dynamics are critical to understanding the behavior of hot nuclear matter formed in very asymmetric nuclear collisions.

II. CALCULATIONS

Transport models, simplified to various degrees, to account for GeV light-ion-induced reactions have included those based on straight-line geometry [17] and intranuclear cascade approaches [16,18,19]. Intranuclear cascade calculations [18] indicate that the conversion of projectile energy into internal heating of the residue occurs quite rapidly, reaching a maximum after a collision time of about 30 fm/c. In order to gain insight into the dynamical evolution of targetlike residues formed in light-ion reactions with heavy nuclei and the mechanism for expansion, we examine here the results of two calculations based on the Boltzmann equation (BUU) [20,21]. These calculations differ in methods and some details of physics input. Both use a soft equation of state and employ relativistic kinematics. The calculation discussed in [20] utilizes a parallel ensemble method, while that discussed in [21] employs a global ensemble method. In [21], gradient terms are included in the expression for energy to account for finite-range effects in the mean field, and further, a lattice Hamiltonian method is used to integrate drift terms in the transport equation. In [20], finite-range effects result from averaging over finite distance in space. Both calculations have been confronted on a number of occasions with different heavy-ion data sets and are in general agreement with each other and experiment as far as single-particle energy spectra and global observables are concerned.

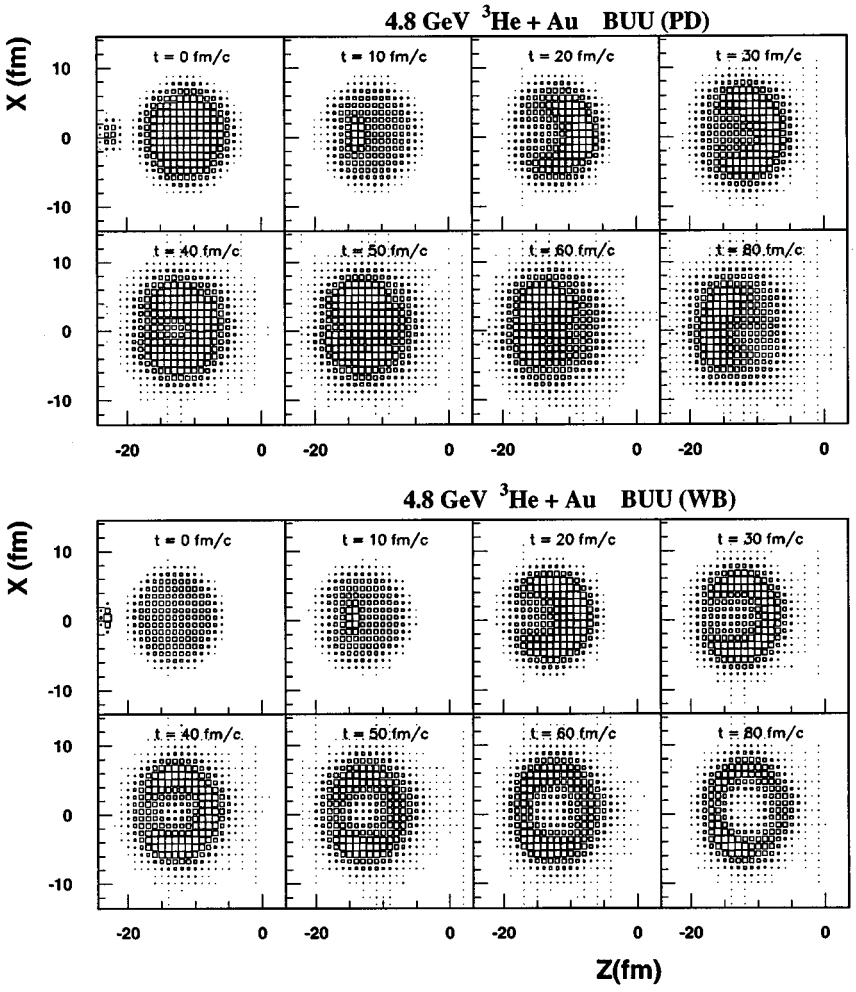

FIG. 1. BUU predictions for central collisions ($b=0$) of 4.8 GeV ^{3}He ions with ^{197}Au nuclei. Shown is the time evolution of two-dimensional invariant density profiles for a plane cut through the center of the reside along the beam axis. Upper figures are from calculations of [21] (P.D.) and lower figures are from calculations based on [20] (W.B.). The Z axis is coincident with the beam direction.

We first compare the two BUU predictions for the 4.8 GeV ^{3}He+^{197}Au reaction. The impact parameter was $b=0$ and 250 test particles/nucleon were used in these calculations. In Fig. 1, two-dimensional density distributions are shown as a function of reaction time for a plane cut through the center of the nucleus along the beam axis (the results are symmetric in azimuthal angle). Results are fairly similar over the first 30 fm/c of reaction time, which accounts for the major part of the energy dissipation and mass loss due to prompt cascade ejectiles. Initially, there is a local buildup of nuclear density ($\sim$30%) as the projectile penetrates into the central region of the target. At reaction times near 20–30 fm/c, a region of depleted density appears in the center of the nucleus, creating an annular shell of nuclear matter. For longer reaction times, the calculation of [20] predicts more viscous behavior, as the hole persists for a length of time approaching that for breakup of the system ($\lesssim$100 fm/c [22]). On the other hand, in the calculation of [21], the hole relaxes after about 50–60 fm/c to an average density of $\rho/\rho_0 \sim 0.4-0.8$ and produces a spheroid-shaped residue, with the major axis perpendicular to the beam axis.

To place the differences in the two codes at times greater than $\sim$50 fm/c in perspective, one must realize that the system is entering a low-density instability region in the phase diagram, characterized by a negative compressibility [23]. In this instability phase, small fluctuations and small differences in predictions between the codes, even of numerical origin, may be amplified exponentially (see also [21]). While this severely limits the predictive power of one-body transport models for the later stages of the reaction, the initial formation of a density depletion is seen in both models and should be considered physical.

Similar results are also obtained in the present BUU calculations for proton-induced reactions in this bombarding energy regime, as well as [24] (using the code of [20]). Earlier intranuclear cascade calculations [16] have also indicated a depleted central density in $p+A$ collisions ($\rho/\rho_0 \approx 0.85$). In Fig. 2, the time evolution of the density distributions is shown for central collisions in the 5 GeV $p+$Au reaction. The results are quite similar to those for ^{3}He projectiles, although the ^{3}He projectile produces a greater density depletion.

A critical question in the coupling of transport codes to models that describe the decay dynamics involves determination of the reaction time at which the fast cascade no longer influences the deposition energy (and related thermal properties) of the excited residue. In Fig. 3, we examine the time evolution of several relevant average quantities: the instantaneous excitation energy per nucleon $\langle E^*/A \rangle$; the maximum density of the system, $\langle \rho_{\max}/\rho_0 \rangle$; the entropy per nucleon, $\langle S/A \rangle$, and mass loss $\langle \Delta A_{\rm res} \rangle$ of the residue. Calculations are shown for 4.8 GeV ^{3}He incident on ^{108}Ag at an impact parameter of 1.8 fm, using the model of [21].

Figure 3 demonstrates that during the first 10–20 fm/c,

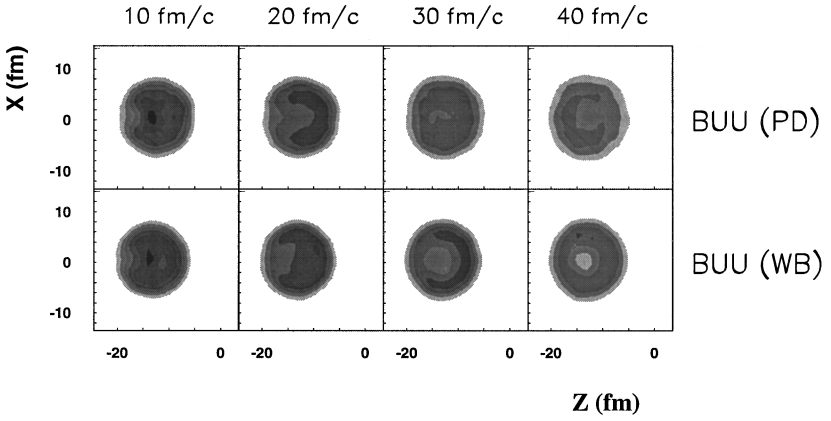

FIG. 2. BUU predictions [20,21] for 5 GeV $p+^{197}$Au reaction, as in Fig. 1.

there is a rapid rise in the excitation energy and entropy per nucleon, accompanied by some density compression. Mass loss, on the other hand, is not significant until a reaction time of about 20 fm/c is reached. Between $\sim$20 and 40 fm/c, the fast cascade produces significant mass loss, causing a rapid decrease in the energy density of the system. At the same time, the entropy per nucleon approaches a maximum value, indicating that the chaotic regime has been reached. By a reaction time of 40 fm/c, the calculation predicts a system for which $\langle E^*/A\rangle \approx 9$ MeV/nucleon, $\langle \rho_{\max}/\rho_0\rangle \simeq 0.65$ and $\langle S/A\rangle \approx 1.3$, corresponding to the region of spinodal decomposition in the ρ-T phase diagram for finite nuclear matter [25]. At longer times, the residue excitation energy, mass and entropy continue to decrease gradually. The density gradually decreases from $\sim$40 to 80 fm/c, suggesting a slight degree of expansion, and then begins to evolve toward normal matter density. It is during this period that density-diffusive fluctuations would be expected to destabilize such systems, leading to nuclear disassembly, or multifragmentation.

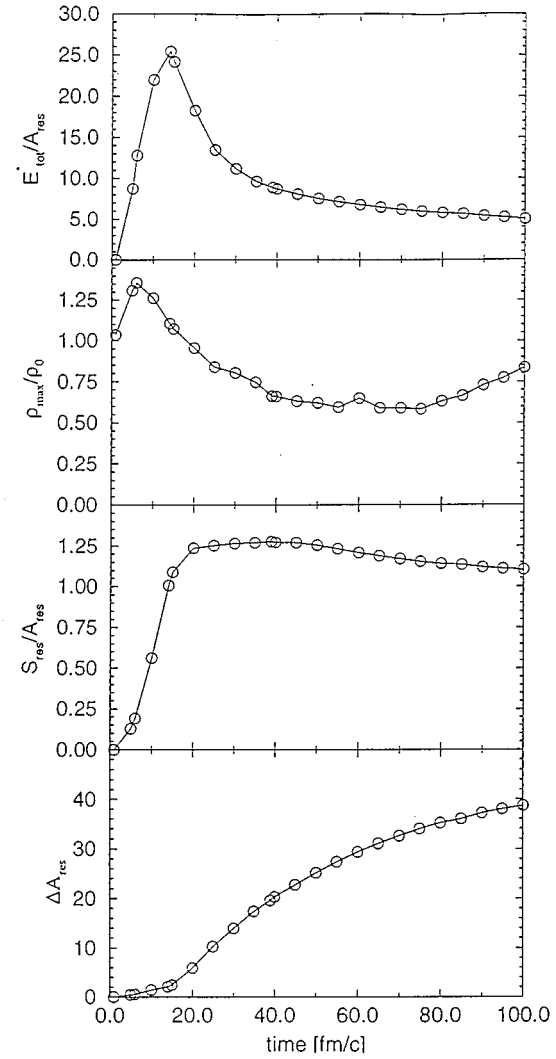

FIG. 3. Evolution of average excitation energy per nucleon, maximum density, entropy per nucleon and residue mass loss in the ^{3}He+^{108}Ag reaction at 4.8 GeV, according to the BUU calculation of [21].

Figure 3 illustrates the difficulty in determining the excitation energy of the system. Both E^* and E^*/A decrease gradually with time for reaction times greater than 40 fm/c. Thus, the question of whether breakup occurs early or late in the evolution of the hot residue is highly relevant to defining its thermal properties.

III. RESULTS

The picture that emerges from the model calculations provides a dynamic mechanism for the destabilization and eventual fragmentation of hot targetlike nuclei produced in light-ion-induced reactions. While little compression is available to drive these processes, the evolution of the shockwavelike momentum front induced by the projectile as it passes through the central region of the nucleus produces several important effects. First, energy is imparted to the target nucleus via N-N scattering and the excitation of Δ and higher resonances, followed by pion reabsorption. During this stage, multiple prompt nucleons are ejected over a time scale that is too short for the nuclear mean field to readjust, thus forming the residue in a state of depleted density. At this point, coalescence involving fast cascade nucleons may produce significant yields of nonequilibrium light fragments. Subsequently, the nucleus is cooled by particle emission, perhaps accompanied by some expansion, until negative pressure develops and the system is driven into the region of diffusive and/or adiabatic instability [25]. The negative pressure limits expansion and causes accumulation of nuclear matter where the density is the largest at a given instant, i.e., in the outer shell of the distribution [21].

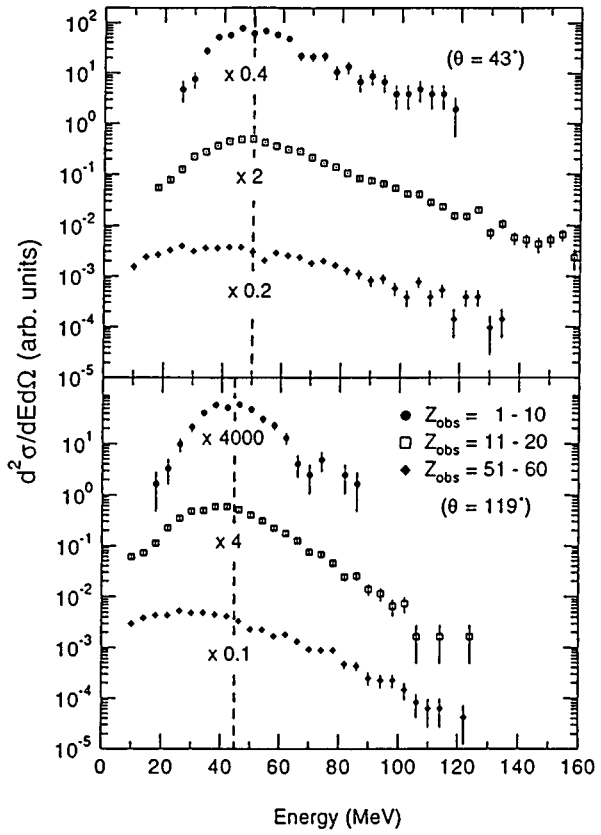

FIG. 4. Kinetic-energy distributions for carbon fragments as a function of collision violence, as determined by total observed charge Z_{obs}, for 4.8 GeV ^{3}He+^{197}Au reaction [7]. The dashed line in each spectrum represents the most-probable-fit peak to the $Z_{\mathrm{obs}}=1-10$ spectrum.

The subsequent relaxation of this bubblelike structure, which must depend sensitively on surface and Coulomb forces, should result in fragmentation of the system with high probability. For example, this could occur in a monopolelike expansion of the shell [22]. A second scenario is the condensation of clusters around the cavitation region, consistent with liquid-vapor coexistence [26,27]. Another possibility is that the shell could implode on the core, followed by an explosion of the system, similar to a blast wave [28]. In all of these pictures, the BUU predictions for the geometry of the system indicate that disintegration occurs from an extended low-density source. This is consistent with the experimental observation of anomalously low kinetic energies for fragments produced in the most violent collisions with light ions [6,7,29], as shown in Fig. 4.

In Fig. 5, we examine the influence of projectile energy on the cavitation process for bombardments of Ag nuclei with 0.9, 1.8, 3.6, and 4.8 GeV ^{3}He ions. Here we show the density distributions along the symmetric axis of the reaction plane as a function of reaction time and relative distance along the beam axis. Results of the two calculations are similar for the first 30–40 fm/c, but diverge at longer times.

At 0.9 GeV, where multifragmentation has been observed experimentally with low probability ($\sim$10 mb) [6], a weak central density depletion develops after about 30 fm/c. With increasing reaction time, the cavity disappears as the nucleus appears to expand and relax to an average density of $\rho/\rho_0\approx 0.8$ at 60 fm/c. Thereafter, the system returns to normal nuclear matter density. As the beam energy increases, the development of the central cavity at times in the vicinity of 30 fm/c becomes more pronounced. The maximum density within the system after that time decreases systematically to rather low values and does not return to nor-

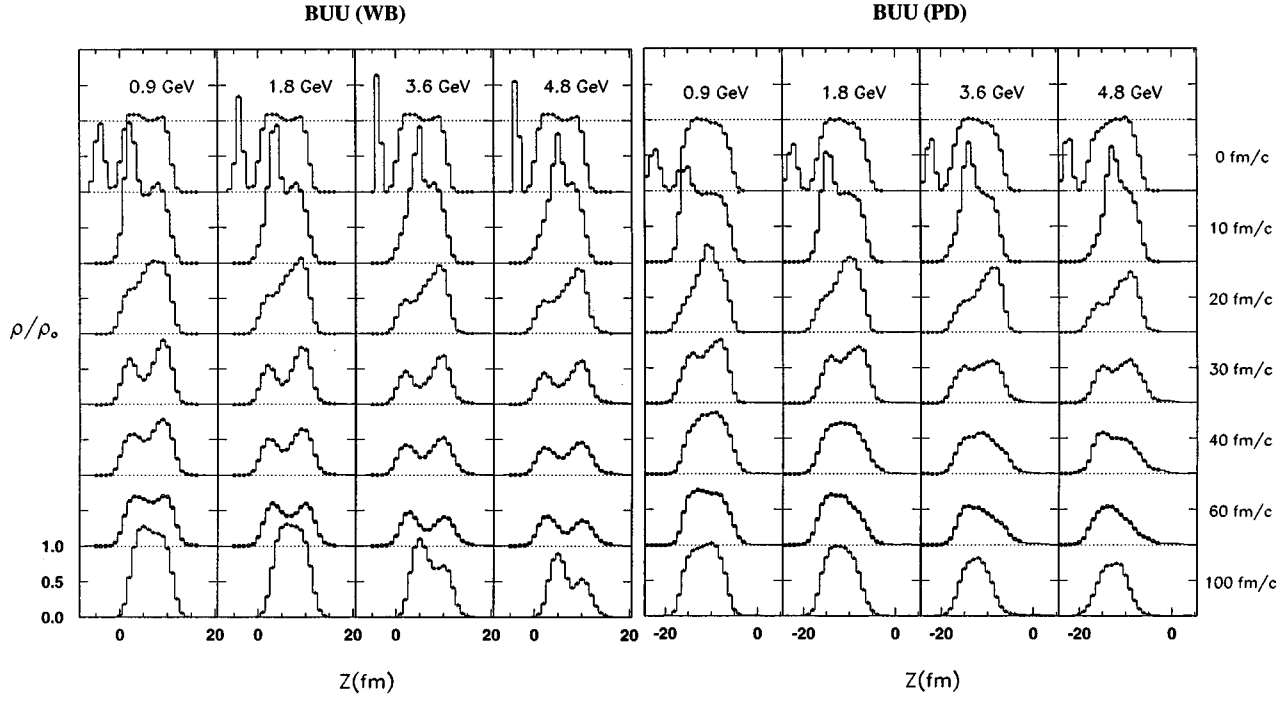

FIG. 5. Evolution of the density profiles along the symmetry axis in the ^{3}He+^{108}Ag reaction at bombarding energies of 0.9, 1.8, 3.6, and 4.8 GeV. Plots at left are from calculations of [20] and those on the right are calculations based on [21]. Reaction time for each row is indicated at the right of the figure.

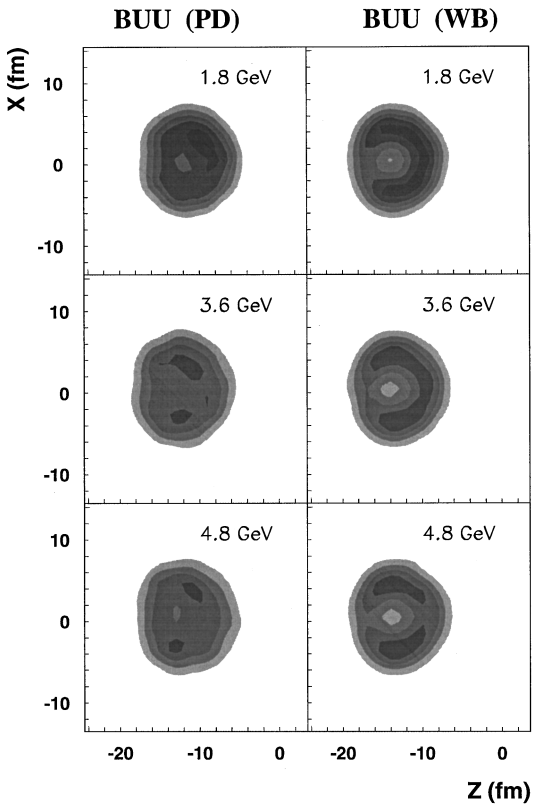

FIG. 6. Density contour plots in the plane containing the symmetry axis at a time 30 fm/c from the start of reaction for the ^{3}He+^{108}Ag system as a function of bombarding energy. Plots at left are predictions based on [20] and those on right are based on [21].

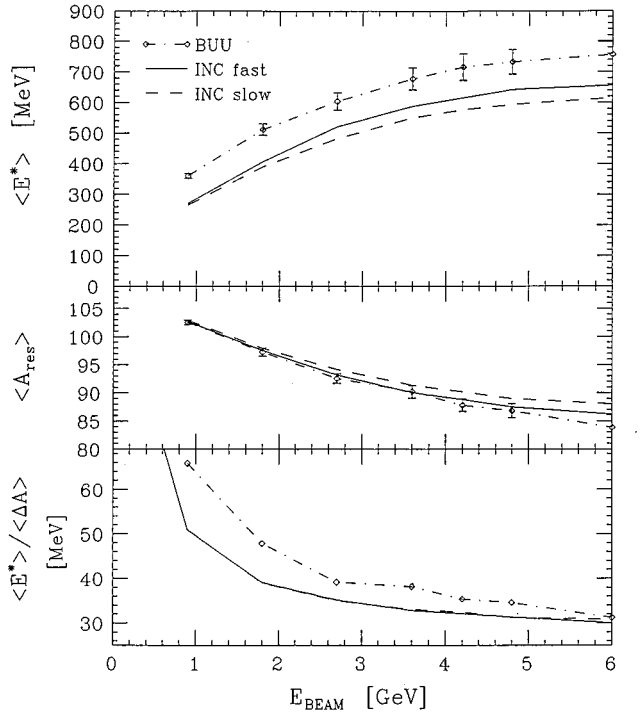

FIG. 7. Average excitation energy (top), residue mass (middle), and excitation energy per cascade nucleon (bottom) in central ^{3}He+^{108}Ag reactions as a function of beam energy. Open points (dot-dashed line) represent values obtained using the BUU code of [21]. The solid line has been obtained with the intranuclear cascade calculation of [19] for the fast rearrangement option in the code and the dashed curve is for the slow rearrangement option.

mal nuclear matter density until times of the order of 100 fm/c. At 4.8 GeV, the region of depleted nuclear density continues to develop as a function of reaction time until it penetrates to the opposite side of the nucleus. Thus, rather than bubble formation, a channel of depleted density is created through the center of the nucleus. This effect becomes more pronounced with increasing projectile energy and mass. As a result, one expects the subsequent disintegration of the system to become independent of bombarding energy once full projectile penetration is achieved. This is the primary explanation for the phenomenon of limiting fragmentation.

This penetration effect is shown more explicitly in Fig. 6 where density patterns at 30 fm/c, slightly greater than the nuclear transit time, are shown for the 1.8, 3.6, and 4.8 GeV ^{3}He+Ag reactions. Once this channel develops, coupled with a saturation in transverse momentum for N-N collisions [30], conversion of dissipated energy into internal excitation energy remains approximately constant. Hence, the deposition energy approaches saturation. This is shown for the ^{3}He+^{107}Ag system in Fig. 7, using the BUU calculation of [21]. Here the average total excitation energy (thermal plus potential), $\langle E^{*}\rangle$, for central collisions ($b=1.8$ fm) is plotted as a function of ^{3}He bombarding energy. As alluded to earlier, the definition of excitation energy in the BUU calculation is time dependent. For the present study, we have chosen the average excitation to correspond to the time interval 40–45 fm/c. At this time, the calculations (Fig. 3) show that (1) the maximum entropy per nucleon of the system is reached, and (2) the rate of decrease of excitation energy per nucleon becomes nearly constant. These seem to be reasonable criteria for defining the onset of thermal behavior. The error bars for the BUU points in Fig. 7 illustrate the range of excitation energy corresponding to 40 fm/c (upper limit) and 45 fm/c (lower limit).

In Fig. 7, the BUU calculations of $\langle E^{*}\rangle$ are also com-

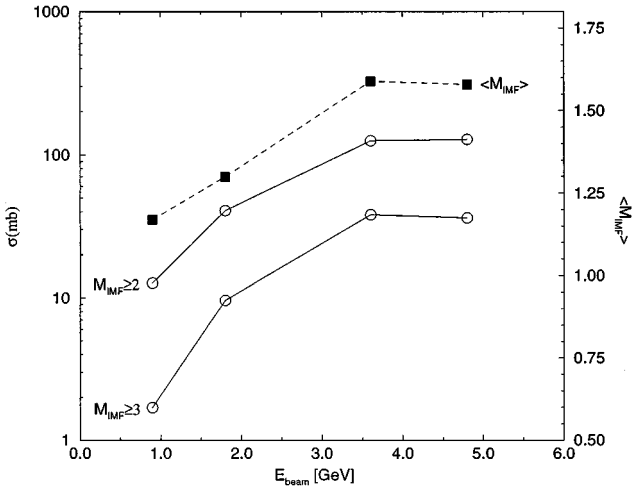

FIG. 8. Average IMF multiplicities (■) and cross sections (○) for IMF multiplicities $M\geq 2$ and $M\geq 3$ as a function of ^{3}He energy [7,31].

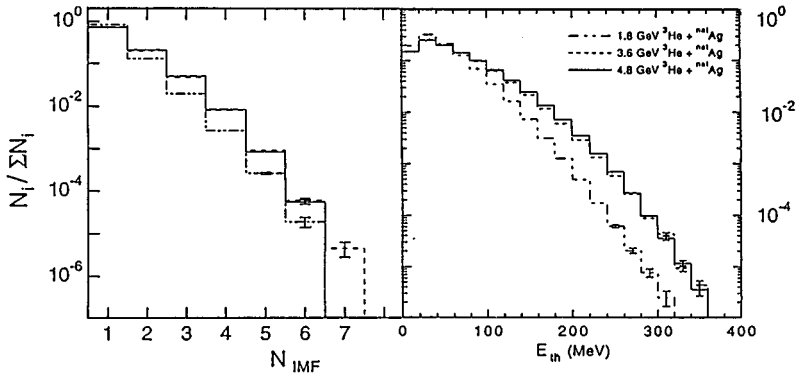

FIG. 9. IMF multiplicity distributions and thermal energy distributions for 1.8, 3.6, and 4.8 GeV ^{3}He+^{nat}Ag reactions [15,32].

pared with the INC code ISABEL [19] for impact parameter $b=1.8$ fm. The upper INC calculation assumes the fast rearrangement option in the code and the lower curve is for slow rearrangement [19]. Maximum excitation energies are achieved with the fast rearrangement option. Within the uncertainties of the calculations, there is good qualitative agreement between the BUU and INC predictions, especially in their approach to excitation energy saturation. The differences in absolute magnitude are most likely due to the fact that the BUU calculation includes both kinetic and potential energy components of the excitation energy, whereas the INC does not include the potential energy. For systems with depleted density, this may be an important difference. The effect of impact parameter on excitation energy saturation should also be noted. As discussed in [15], the INC model predicts that as the impact parameter increases, the onset of excitation energy saturation occurs at progressively lower bombarding energies. The reader should also be reminded that the INC predicts broad distributions in E^* and ΔA, whereas the BUU produces only a single average value. For all cases, the predicted residue mass is quite similar, as is the average excitation energy per cascade nucleon lost by the residue. The behavior of the energy converted into deposition energy per cascade nucleon suggests that beyond about 2 GeV ^{3}He energy, this quantity becomes nearly independent of bombarding energy. The rise at low energy reflects the increased probability for thermalization of the projectile energy.

The model calculations are in accord with experimental excitation function data for the ^{3}He+^{nat}Ag system, which indicate a saturation in deposition energy near 4 GeV bombarding energy [15]. This is shown in Figs. 8 and 9 for several variables, including the IMF probabilities and multiplicity distributions [7,31] and the distribution of total observed thermalized energy per event (the thermalized energy is the total kinetic energy in an event after nonequilibrium ejectiles have been removed [15,32]). The data at 3.6 and 4.8 GeV are nearly identical for all variables in Figs. 8 and 9 as well as other observables believed to be strongly correlated with excitation energy deposition, such as thermal charged particle multiplicities and total observed ejectile charge [15,32]. This interpretation is also consistent with the observation of limiting fragmentation [8] and constant IMF charge distributions for energetic light-ion-induced reactions [4,6].

Finally, another aspect of the BUU density profiles relates to the observed sideways peaking of fragment angular distributions near $\sim$10 GeV in $p+A$ reactions [10,11]. In the BUU simulations, this comes about in two ways, both of which involve significant transverse momentum transfer. First, for midcentral collisions, the cavity that forms in the wake of the projectile momentum front erodes away one side of the target, leaving a highly excited residue with a significant transverse momentum component. This is illustrated in Fig. 10 for the 4.8 GeV ^{3}He+^{197}Au reaction with the code of [20]. Here the impact parameter is $b=4.6$ fm. Clearly, residues formed in such interactions will experience preferential emission in a direction perpendicular to the beam axis, thus producing the observed sideways peaking.

Second, for more central collisions, conditions for emission of fragments transverse to the beam direction develop once a channel of highly depleted density is formed, as suggested by Fig. 6. In this case, not only is there a significant momentum component perpendicular to the beam axis, but the Coulomb field of the system favors focusing towards 90° in the residue system. If fluctuations in the reaction dynamics favor the formation of only two fragments early in the reaction time, a special situation develops, i.e., a cleaving of the nucleus along a plane [17]. In this case, the scission configuration is more compact than for the distended shapes characteristic of normal binary fission events, resulting in

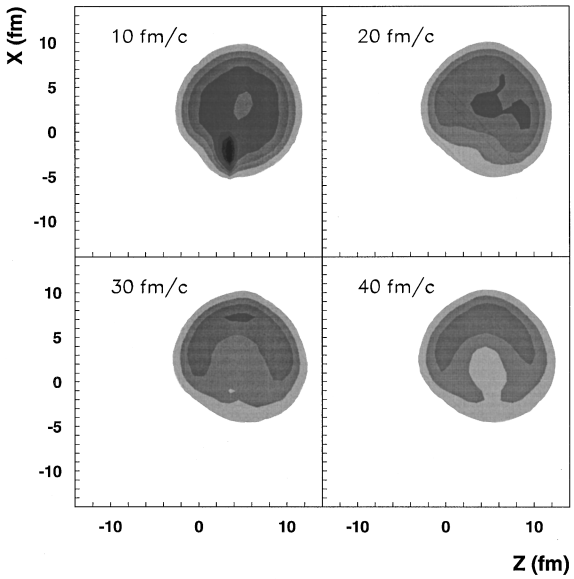

FIG. 10. Two-dimensional BUU profiles for a midcentral impact parameter of $b=4.6$ fm for the 4.8 GeV ^{3} He+^{197}Au reaction, using the model of [20].

greater Coulomb repulsion and more energetic fragments. In addition, mass loss during the fast cascade should produce lighter than normal fragments. A similar interpretation was proposed by Wilkins *et al.* [12] to explain observation of a binary fissionlike component with anomalously high kinetic energies and lighter than average masses in the 12 GeV $p+^{238}$U reaction. Similar arguments have been used by Hüfner [17] to explain these results.

IV. CONCLUSIONS

The picture that emerges from these BUU investigations of the reaction dynamics suggests a time-dependent model of multifragmentation, similar to that proposed by Friedman [22] and Nörenberg [33]. In the schematic model of Friedman, multifragmentation is viewed as the consequence of a monopole expansion of the excited nucleus driven by thermal pressure. During expansion, nucleons and fragments can be emitted from the hot system. In general, this process is viewed as a volume increase of a system with an approximately constant number of constituent nucleons. The time dependence of the BUU calculations investigated here yields an analogous result, except that the dilute phase is at least partially attained by the rapid removal of multiple nucleons/coalesced fragments from an approximately constant volume (since there is insufficient time for significant collective behavior). The success of a hybrid model based on an intranuclear cascade [19] expanding emitting source [22] calculation in fitting intermediate mass fragment multiplicities, energy spectra and large-angle velocity correlations [7,34] may have its origin in this correspondence.

In summary, we have examined results from two separate BUU calculations to investigate the dynamics and energy deposition in light-ion-induced reactions. The results indicate that at bombarding energies of several GeV, central collisions produce a depleted region of nuclear density in the center of the target nucleus at reaction times in the interval 20–50 fm/c. This bubblelike structure may provide a mechanism to account for expansionlike behavior of nuclei formed in light-ion-induced reactions, leading to eventual multifragmentation and characterized by very low-energy fragments [7]. This may resolve the discrepancy between experiment and previous BUU/QMD calculations [35,36], where purely thermal heating of uniform spherical nuclei resulted in little expansion. In two-step models of multifragmentation, the depleted density of the hot residue needs to be considered in the application of the breakup mechanism.

At ^{3}He energies near 4 GeV for Ag targets, the BUU model predicts that the projectile collision front will penetrate the target nucleus, leading to a saturation of deposition energy beyond this bombarding energy. This saturation is also predicted by INC calculations. In general, there is agreement between the two models, except that the omission of potential energy in calculating the excitation energy with the INC model leads to somewhat lower values for density-depleted systems. The predicted saturation in energy deposition is consistent with numerous observations of energy-independent behavior in the properties of target residues formed in such reactions. Finally, the simulations can qualitatively account for the transition from forward to sideways peaking in the fragment angular distributions and detection of unusually energetic fission-like phenomena over the energy regime 1–10 GeV.

ACKNOWLEDGMENTS

We thank W. A. Friedman, H. Müller, and B. D. Serot for discussions relevant to this work, as well as David Ginger for assistance with preparing the manuscript. This work was supported by the U.S. Department of Energy (Grant No. DEFG02-88ER.40404A000) and the National Science Foundation (Grant No. PHY-9403666). Partial support from the Presidential Faculty Fellowship Program (W.B.) is also acknowledged, as is the Nuclear Theory Institute at the University of Washington.

[1] J. Hudis, in *Nuclear Chemistry*, edited by L. Yaffe (Academic Press, New York, 1968), p. 169.
[2] W. G. Lynch, Annu. Rev. Nucl. Part. Sci. **37**, 439 (1987).
[3] S. B. Kaufman and E. P. Steinberg, Phys. Rev. C **22**, 167 (1980).
[4] N. T. Porile *et al.*, Phys. Rev. C **39**, 1914 (1989).
[5] Review of Particle Properties, Phys. Rev. D **50**, 1336 (1994); see also J. P. Meyer, Astron. Astrophys. Suppl. **7**, 417 (1972); G. J. Igo, Rev. Mod. Phys. **50**, 523 (1978).
[6] S. J. Yennello *et al.*, Phys. Rev. C **48**, 1092 (1993).
[7] K. Kwiatkowski *et al.*, Phys. Rev. Lett. **74**, 3756 (1995).
[8] G. Rudstam, Z. Naturforsch. Teil A **21a**, 1027 (1966).
[9] J. L. Wile *et al.*, Phys. Rev. C **45**, 2300 (1992).
[10] L. P. Remsberg and D. G. Perry, Phys. Rev. Lett. **35**, 361 (1975).
[11] D. R. Fortney and N. T. Porile, Phys. Rev. C **21**, 2511 (1980); **22**, 670 (1980).
[12] B. D. Wilkins, S. B. Kaufman, and E. P. Steinberg, Phys. Rev. Lett. **43**, 1080 (1979).
[13] K. Nakai, Nucl. Phys. **A418**, 163c (1994).
[14] I. N. Mishustin, V. N. Russkikh, and L. M. Satorov, Nucl. Phys. **A494**, 595 (1989); G. N. Agakishiev *et al.*, Sov. J. Phys. **49**, 300 (1989).
[15] K. B. Morley *et al.*, Phys. Lett. B **355**, 52 (1995).
[16] V. Barashenkov, A. S. Iljinov, and V. D. Toneev, Sov. J. Nucl. Phys. **13**, 422 (1971); Actra Phys. Pol. B **1**, 219 (1973); V. Toneev and K. K. Gudina, Nucl. Phys. **400**, 173c (1982).
[17] J. Hüfner, Phys. Rep. **125**, 131 (1985); S. Bohrmann, J. Hüfner, and M. C. Nemes, Phys. Lett. **120B**, 59 (1983); J. Hüfner and H. M. Sommerman, Phys. Rev. C **27**, 2090 (1985).
[18] J. Cugnon, D. Kinet, and J. Vandermeulen, Nucl. Phys. **A379**, 553 (1982); J. Cugnon, *ibid.* **462**, 751 (1987).
[19] Y. Yariv and Z. Fraenkel, Phys. Rev. C **24**, 488 (1981).
[20] W. Bauer, G. F. Bertsch, W. Cassing, and U. Mosel, Phys. Rev. C **34**, 2127 (1986); W. Bauer, Phys. Rev. Lett. **61**, 2534 (1988); W. Bauer, C. K. Gelbke, and S. Pratt, Annu. Rev. Nucl. Part. Sci. **42**, 77 (1992).
[21] P. Danielewicz and G. F. Bertsch, Nucl. Phys. **A533**, 712

(1991); P. Danielewicz, Phys. Rev. C **51**, 716 (1995).
[22] W. A. Friedman, Phys. Rev. C **42**, 667 (1990).
[23] W. Bauer, G. F. Bertsch, and H. Schultz, Phys. Rev. Lett. **69**, 1888 (1992).
[24] E. Norbeck *et al.*, *Proceedings of 9th High Energy Heavy-Ion Study*, Berkeley (LBL Report 35984, 1994), p. 102.
[25] H. Müller and B. D. Serot, Phys. Rev. C **52**, 2072 (1995).
[26] R. J. Lenk and V. R. Pandharipande, Phys. Rev. C **34**, 177 (1986); T. J. Schlagel and V. R. Pandharipande, *ibid.* **36**, 162 (1987).
[27] S. Pratt, Phys. Rev. A **42**, 1447 (1990); S. Pratt *et al.*, Phys. Lett. B **349**, 261 (1995).
[28] P. J. Siemens and J. O. Rasmussen, Phys. Rev. Lett. **42**, 880 (1979).
[29] A. M. Poskanzer, G. W. Butler, and E. K. Hyde, Phys. Rev. C **3**, 882 (1971); **4**, 1759 (1971); G. D. Westfall, R. G. Sextro, A. M. Poskanzer, A. M. Zebelman, G. W. Butler, and E. K. Hyde, *ibid.* **17**, 1368 (1978); A. I. Warwick, H. H. Wieman, H. H. Gutbrod, M. R. Maier, J. Péter, H. G. Pitter, H. Stelzer, and F. Welk, *ibid.* **27**, 1083 (1983).
[30] G. Bertsch, in *Nuclear Physics with Heavy Ions and Mesons*, edited by R. Balian and G. Ripka (North-Holland, Amsterdam, 1978), Vol. 1, p. 251.
[31] E. Renshaw Foxford *et al.*, submitted to Phys. Rev. C.
[32] K. B. Morley *et al.*, submitted to Phys. Rev. C.
[33] G. Papp and W. Nörenberg, GSI Report 95-30; Z. He, J. Wu, and W. Nörenberg, Nucl. Phys. **A489**, 421 (1988).
[34] V. E. Viola *et al.*, in *Proceedings of the ACS Symposium in Honor of J. B. Natowitz*, edited by N. Namboodiri and G. Nebbia (World Scientific, Singapore, to be published).
[35] G. Batko and J. Randrup, Nucl. Phys. **A563**, 97 (1993).
[36] L. de Paula, J. Nemeth, B.-H. Sa, S. Leray, C. Ngô, H. Ngô, S. R. Souza, and Y.-M. Zheng, Phys. Lett. B **258**, 251 (1991).